# Zero-degree cross sections for the $^7$Li($p,n$)$^7$Be(g.s.+0.43-MeV) reaction in the energy range 80–795 MeV

T. N. Taddeucci,[a] W. P. Alford,[j] M. Barlett,[i] R. C. Byrd,[a] T. A. Carey,[a] D. E. Ciskowski,[i] C. C. Foster,[b] C. Gaarde,[c] C. D. Goodman,[b] C. A. Goulding,[a] E. Gülmez,[g] W. Huang,[b] D. J. Horen,[d] J. Larsen,[c] D. Marchlenski,[f] J. B. McClelland,[a] D. Prout,[h] J. Rapaport,[e] L. J. Rybarcyk,[a] W. C. Sailor,[a] E. Sugarbaker,[f] and C. A. Whitten, Jr.[g]

[a]*Los Alamos National Laboratory, Los Alamos, New Mexico 87545*
[b]*Indiana University, Bloomington, Indiana 47405*
[c]*Niels Bohr Institute, Copenhagen, Denmark*
[d]*Oak Ridge National Laboratory, Oak Ridge, Tennessee 37830*
[e]*Ohio University, Athens, Ohio 45701*
[f]*Ohio State University, Columbus, Ohio 43210*
[g]*University of California, Los Angeles, California 90024*
[h]*University of Colorado, Boulder, Colorado 80309*
[i]*University of Texas, Austin, Texas 78712*
[j]*University of Western Ontario, London, Ontario, Canada N6A 3K7*

(Received 27 December 1989)

Differential-cross-section distributions for the $^7$Li($p,n$)$^7$Be(g.s.+0.43-MeV) reaction have been measured for $E_p$=80, 120, 160, 200, 494, 644, and 795 MeV. These distributions have been integrated and normalized to independent values for the total cross section obtained from parametrizations of $^7$Li($p,n$) activation measurements. Zero-degree cross sections obtained from this normalization are reported.

## I. INTRODUCTION

Detection of fast neutrons with good energy resolution is necessarily accomplished with detectors that are significantly less than 100% efficient. Some technique of determining the detector efficiency is therefore required in order to derive properly normalized cross sections from measured neutron yields. The detector efficiency can be determined either by sophisticated Monte Carlo simulations[1,2] or by direct measurement with tagged neutrons.[3,4] Alternately, a quantity proportional to the product of the efficiency and other fixed experimental parameters (such as solid angle, neutron attenuation factor, current-integrator scale, etc.) can be determined by normalizing to a reaction with known cross section.[5,6]

The ($p,n$) reaction on $^7$Li leading to the ground state and first excited state (0.43 MeV) in $^7$Be is a convenient reaction to employ for normalization purposes. This reaction proceeds primarily through $L=0$ angular-momentum transfer and is therefore peaked at a scattering angle of 0°. The large 0° cross section for this reaction ($\simeq$35 mb/sr lab) and the small atomic weight of $^7$Li combine to yield relatively large neutron fluxes for a given beam intensity and target thickness. In addition, there are no other low-energy-loss $^7$Li($p,n$) channels with appreciable cross section at 0°; the high-energy flux at this neutron production angle is therefore almost monoenergetic.

There are no particle-emission stable states in $^7$Be above the first excited state. Residual $^7$Be nuclei produced by bombarding $^7$Li with protons must therefore have been produced by ($p,n$) transitions to the ground state or first excited state. [It is assumed that alternate production channels, such as ($p,p'\pi^-$), will contribute negligibly because of the large momentum transfer involved.] The total cross section for ($p,n$) transitions to these two levels can therefore be measured by counting the number of residual radioactive $^7$Be nuclei. The total cross section can also be obtained, to within an overall normalization factor, by integrating the differential-cross-section angular distribution for the (g.s.+0.43-MeV) transition. Comparison of the two results gives the proper normalization factor for the differential-cross-section distribution,[7] and therefore yields the zero-degree differential cross section independent of any knowledge of the neutron-detector efficiency.

In this paper we present differential-cross-section distributions for the $^7$Li($p,n$)$^7$Be (g.s.+0.43-MeV) reaction measured at bombarding energies between 80 and 795 MeV. These distributions have been normalized by comparison to total cross sections measured by the activation technique discussed above. Suitable parametrizations of the activation cross sections have been used to extrapolate to energies where activation measurements have not yet been made. Zero-degree cross sections obtained by this normalization procedure are presented. These zero-degree cross sections should be useful standards for normalizing future ($p,n$) data and for use in neutron-detector efficiency measurements.

 

## II. EXPERIMENTAL SUMMARY

Angular distributions for the reaction $^7$Li$(p,n)^7$Be (g.s. +0.43 MeV) have been measured for nominal bombarding energies of 80, 120, 160, and 200 MeV at the Indiana University Cyclotron Facility (IUCF) and for bombarding energies of 494, 644, and 795 MeV at the Clinton P. Anderson Meson Physics Facility (LAMPF) in Los Alamos. The IUCF data were obtained in the period 1979–1981. The LAMPF data were obtained recently with the new Neutron Time-of-Flight (NTOF) Facility[8] during the period 1987–1988.

The IUCF data were obtained with the beam-swinger facility[9] and double-ended plastic (NE102) scintillation detectors. The detectors were operated in the tilt-angle mode to obtain time-of-flight measurements of the outgoing neutron energy with subnanosecond resolution.[10] Coverage of angles up to 48° was obtained by placing detectors in two fixed stations. One station was on the 0° line with respect to the undeflected beam and the other on the 24° line. The uncertainty in the scattering angle is estimated to be $\leq 0.1°$. The flight path varied from 70 to 90 m. The targets were rolled Li metal enriched to $>99\%$ in $^7$Li. The areal density of each target was in the range 15–38 mg/cm$^2$. Beam current was monitored with an external split Faraday cup.

The LAMPF data were obtained with position-sensitive mean-timed liquid scintillation detectors that can also function as a neutron polarimeter.[8] Typical neutron time-of-flight resolution was about 0.6 ns, including beam contributions. The data were obtained in three separate experimental runs, each at a different flight path.

The first measurements were made with polarized beam during the commissioning phase of the NTOF facility.[8] The beam energy was 494 MeV, the flight path was 81 m, and the angular range covered was 0°–26°. The overall energy resolution was approximately 3.0 MeV. The period between beam bursts was 99.38 ns. Frame-overlap neutrons (slower neutrons from preceding beam bursts) were rejected by operating the detector system in coincidence mode. In this mode of operation, the incident neutrons are required to undergo either elastic $(n,n)$ or charge-exchange $(n,p)$ scattering with protons in the scintillator. The velocity of the scattered neutron or proton is then measured by time of flight between two detector planes separated by approximately 1.7 m. This second velocity measurement provides sufficient information to reconstruct the event kinematically and thereby distinguish high-energy neutrons from low-energy neutrons with the same apparent time of flight (i.e., flight time modulo the beam-burst period).

A second set of cross sections was measured with a polarized beam of 644-MeV protons and a neutron flight path of 170 m. Data were obtained at two angles (0° and 6°) with a resolution of about 2.5 MeV. The beam-burst period was 99.38 ns and the detectors were operated in coincidence mode.

The third set of cross sections was measured with unpolarized beam and a flight path of 617 m. Three beam energies were used: 494, 644, and 795 MeV, with overall energy resolution of approximately 1.2, 1.2, and 2.0 MeV, respectively. The period between beam bursts was 4.969 $\mu$s. The detectors were operated in singles mode. For this beam-burst period and flight path, the energy of frame-overlap neutrons is in the range 35–38 MeV. These neutrons are easily rejected by a simple pulse-height cut. In addition, the attenuation of these lower-energy neutrons is approximately a factor of five larger than that for the higher-energy neutrons of interest. The 494-, 644-, and 795-MeV data spanned the angular range 0°–9° in 1° steps. At 795 MeV, measurements were also made at 12°, 16°, and 20°.

The first set of 494-MeV data required corrections ($\leq 0.5°$) to some of the measured scattering angles because of backlash in the positioning of beam-monitoring devices. At larger angles ($>9°$) it was possible to correct the scattering angle to an uncertainty of about $\pm 0.1°$ by using the observed kinematic shift of the neutron group corresponding to $^7$Be (g.s.+0.43). The angle readout problems were fixed for the subsequent sets of data. The scattering angle uncertainty for these later data is estimated to be $<0.1°$.

The target used in all the LAMPF measurements consisted of enriched Li metal packed into an aluminum frame. The thickness was 1 cm. Relative beam intensity was measured with secondary-emission monitors upstream of the target. The long flight path (617 m) measurements require corrections for changes in the neutron attenuation in air due to temperature and barometric pressure changes. The largest of these relative corrections is 3.8%. Corrections in the range 1–2 % are more typical.

## III. PARAMETRIZATION OF THE TOTAL CROSS SECTION

The total cross section $\sigma_T$ for the reaction $^7$Li$(p,n)^7$Be (g.s.+0.43 MeV) can be measured by irradiating a $^7$Li target with a known proton flux and then counting the $\gamma$ rays that follow the $^7$Be$\rightarrow^7$Li (0.478 MeV) electron capture decay in the activated target. Measurements have been reported by Valentin *et al.*[11] for $E_p=155$ MeV, Schery *et al.*[7] for $25\leq E_p\leq 45$ MeV, Ward *et al.*[12] for $60\leq E_p\leq 200$ MeV, and D'Auria *et al.*[13] for $60\leq E_p\leq 480$ MeV. The results of measurements made with pure $^7$Li metal targets are displayed in Fig. 1. The approximate $1/E$ energy dependence for this cross section was first noted by Ward *et al.*,[12] who fit the data from $25\leq E_p\leq 200$ MeV to the functional form

$$\ln(\sigma_T)=a+b\ln(E_p)\ . \tag{1}$$

A similar fit was reported by D'Auria *et al.*[13] for $60<E_p<480$ MeV. A global fit, using the data of Schery *et al.*,[7] Valentin *et al.*,[11] and D'Auria *et al.*,[13] yields

$$\begin{aligned} a&=7.02\pm 0.05\ , \\ b&=-1.13\pm 0.01 \end{aligned} \tag{2}$$

for $25<E_p<480$ MeV. An alternate way of parametrizing the energy dependence of this cross section can be derived from the expression relating the total cross section to the angle-integrated differential cross section:

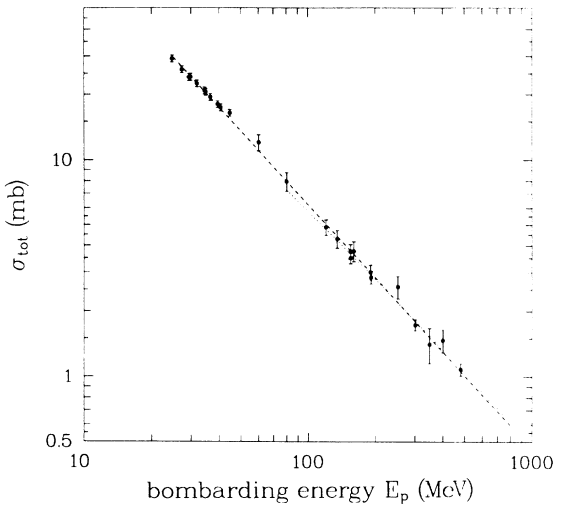


FIG. 1. Total cross section for the $^7$Li$(p,n)^7$Be (g.s.+0.43-MeV) reaction. The dashed line corresponds to the parametrization of Eq. (1). The dotted line assumes a constant value for the momentum-transfer integral $I_q$ [Eq. (5)].

$$\sigma_T = 2\pi \int_0^{\pi} \sigma(\theta) \sin\theta \, d\theta \ . \tag{3}$$

This expression can also be written as

$$\sigma_T = \frac{2\pi}{k_i k_f} \int q\sigma(q) dq \ , \tag{4}$$

where $k_i$, $k_f$, and $q$ are the initial and final wave numbers and the momentum transfer in the center-of-mass frame. The limits on the integral go from $q_{\min} = k_i - k_f$ to $q_{\max} = k_i + k_f$. The momentum-transfer integral

$$I_q = \int q\sigma(q) dq \tag{5}$$

extracted from the activation total-cross-section data is displayed in Fig. 1. The data in Fig. 2 are consistent with a constant value of

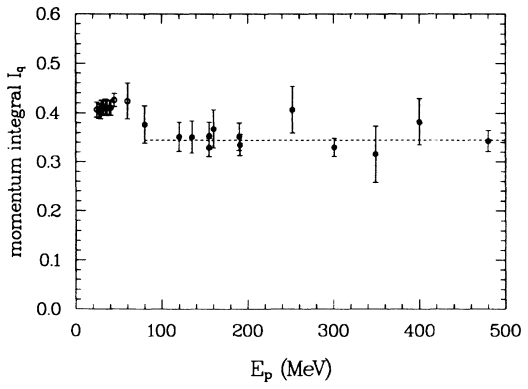


FIG. 2. Values for the momentum-transfer integral $I_q$ extracted from the activation cross sections of Fig. 1. The dashed line corresponds to a constant value of $I_q = 0.345 \pm 0.008$.

$$I_q = 0.345 \pm 0.008 \tag{6}$$

for energies $E_p > 80$ MeV. A linear fit of the form $I_q = a + bE_p$ yields an insignificant result for the slope parameter $b$. The chi squared per degree of freedom is marginally better for the parametrization of Eqs. (4)–(6) than for that of Eq. (1) when applied only to the data for $E_p > 80$ MeV. A constant value for $I_q$ will result if the c.m. momentum-transfer distribution is invariant with bombarding energy. An approximate invariance was recently noted by Watson *et al.*[14] and is also seen in the data presented in the next section. Compensating differences in the $\sigma(q)$ distribution can also lead to a constant value for $I_q$, so the result of Eq. (6) is not sufficient to guarantee an invariant integrand (momentum-transfer distribution). However, the qualitative similarity of the distributions for all energies $E_p > 80$ MeV indicates that any shape differences are small.

The activation cross sections used here are based upon the previously accepted value of (10.4±0.1)% for the $^7$Be(ε)$^7$Li(0.48-MeV) branching ratio.[15] Reports that this value may be erroneous stimulated many new measurements about six years ago. The weighted average including these new measurements is[16] (10.45±0.04)%. This updated value is close enough to the previous one that we have not corrected the activation data to reflect the new measurements.

## IV. INTEGRATION OF THE EXPERIMENTAL DISTRIBUTIONS

The momentum-transfer distribution $q\sigma(q)$ at each energy was integrated by summing the area between successive data points. The areal elements were computed using Gaussian interpolation between values of $\sigma(q)$. This technique is especially appropriate at low momentum transfer[17] ($q < 0.7$ fm$^{-1}$) and beyond this range the difference between this type of interpolation and exponential interpolation contributes negligible uncertainty to the integral. The area beyond the last measured value of $\sigma(q)$ was estimated by integrating an exponential function

$$\sigma_E(q) = \sigma_0 \exp(-qR) \ , \tag{7}$$

where the slope parameter $R = 3.0 \pm 0.1$ is the weighted averaged of the values obtained from least-squares fits to the distributions extending to $q = 1.9$ fm$^{-1}$ or larger (i.e., for $E_p = 120$, 160, 200, 494, and 795 MeV). This extrapolated area is significant only for the 80-, 120-, and 644-MeV distributions, which extend to 0.891, 1.941, and 1.014 fm$^{-1}$, respectively. The extrapolated area represents 21.6% of the total at 80 MeV, 1.7% of the total at 120 MeV, and 17.7% of the total at 644 MeV. The contribution is less than 1% for all other energies.

The estimated uncertainty in each integrated distribution includes the effects of the statistical uncertainty for each data point, an additional 2% systematic uncertainty on each data point (attributed to current integration, live-time correction, etc.), and the estimated uncertainty in the extrapolated area.

The integrated distributions were normalized to the ac-

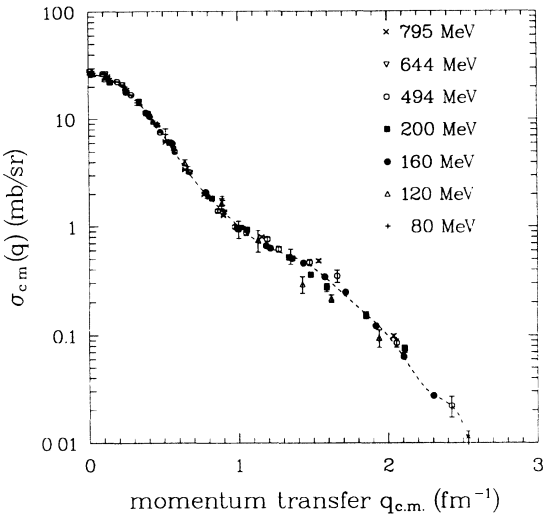


FIG. 3. Differential cross sections for the $^7$Li($p,n$)$^7$Be (g.s. +0.43-MeV) reaction between 80 and 795 MeV. The distributions are normalized assuming a constant momentum integral $I_q$. The dashed line represents a Bessel function fit with nine terms [Eq. (9)].

tivation cross sections as parametrized in Sec. III. The uncertainty in the total cross section obtained from the parametrization of Eq. (1) can be estimated from the covariance matrix of the least-squares fit. This uncertainty is 3.8% at 795 MeV and only 1.2% at 80 MeV. By comparison, the constant-$I_q$ assumption yields an uncertainty of 2.2%. The distributions normalized to the constant-$I_q$ parametrization are displayed in Figs. 3 and 4.

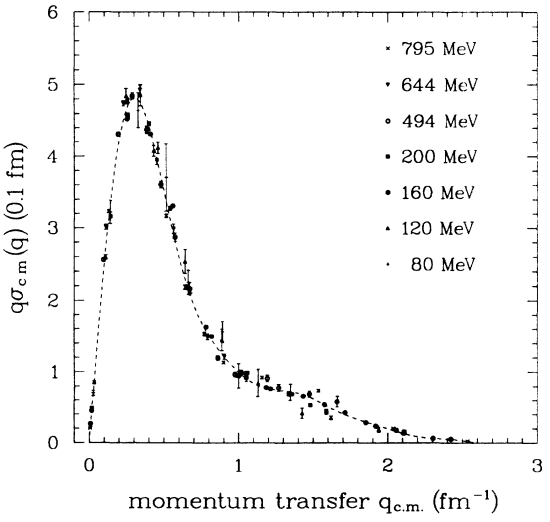


FIG. 4. Distribution of $q\sigma(q)$ from Fig. 3. The dashed line represents a Bessel function fit with nine terms [Eq. (12)].

## V. ZERO-DEGREE DIFFERENTIAL CROSS SECTION

The differential cross section section $\sigma_0$ corresponding to $q=0$ was obtained from each normalized distribution by performing a least-squares Gaussian fit to the low-momentum-transfer region, where the distribution is well described by[17]

$$\sigma(q)=\sigma_0 \exp\left[-q^2\frac{\langle r^2\rangle}{3}\right] . \quad (8)$$

Values for the mean-square radius (msr) $\langle r^2\rangle$ determined by fitting each distribution for $q<0.5$ fm$^{-1}$ are displayed in Fig. 5. The low-$q$ distributions and the corresponding fits are shown in Figs. 6 and 7.

The main contributions to $\langle r^2\rangle$ are from the transition density and the effective interaction. The energy-dependent msr for the central isovector spin-flip interaction has been obtained from the $t$-matrix parametrization of Franey and Love.[18] An analysis of $^7$Li($e,e'$) transverse form factors for the unresolved g.s.+0.478-MeV doublet yields an msr of 7.29±0.81 fm$^2$ for the magnetization density.[19] Similarly, the msr for the charge density is[20] 5.71±0.14 fm$^2$. These values have been added to the msr for the effective interaction to produce the solid and dashed lines, respectively, in Fig. 5. Distortion effects have been neglected in this comparison. All of the energy dependence in the two calculated curves comes from the effective interaction. The minor contribution from the central non-spin-flip interaction has been neglected. Also, an analysis of electron scattering data for the ground state and resolved 0.478-MeV level yields somewhat larger values for the two ground-state radii.[21] In spite of the obvious limitations, this simple calculation does a good job of reproducing the trend of the data. A more quantitative analysis is beyond the scope of this paper.

The range of momentum transfer over which to fit the data must be carefully chosen to avoid contributions from $L>0$ angular-momentum transfer. A range that is

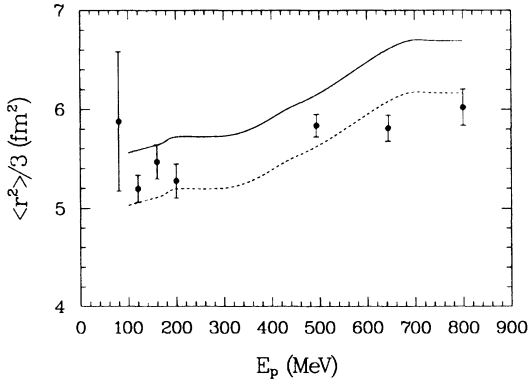


FIG. 5. Mean-squared radius $\langle r^2\rangle$ extracted from the $^7$Li($p,n$) cross-section distributions. [See Eq. (8).] The solid and dashed lines represent calculations based upon the mean-squared radius of the magnetization density and charge density, respectively.

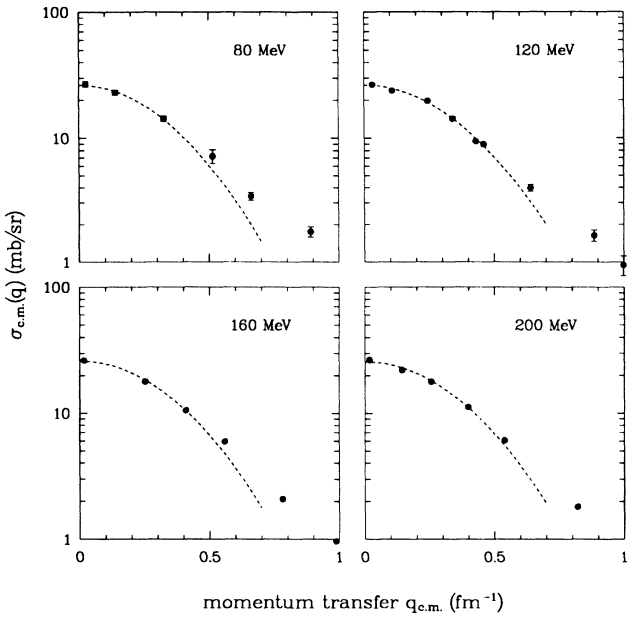


FIG. 6. Low-momentum-transfer differential cross sections for the $^7$Li$(p,n)^7$Be (g.s.+0.43-MeV) reaction at 80, 120, 160, and 200 MeV. The data were obtained at IUCF. The dashed lines correspond to Gaussian least-squares fits to the data for $q \leq 0.5$ fm$^{-1}$.

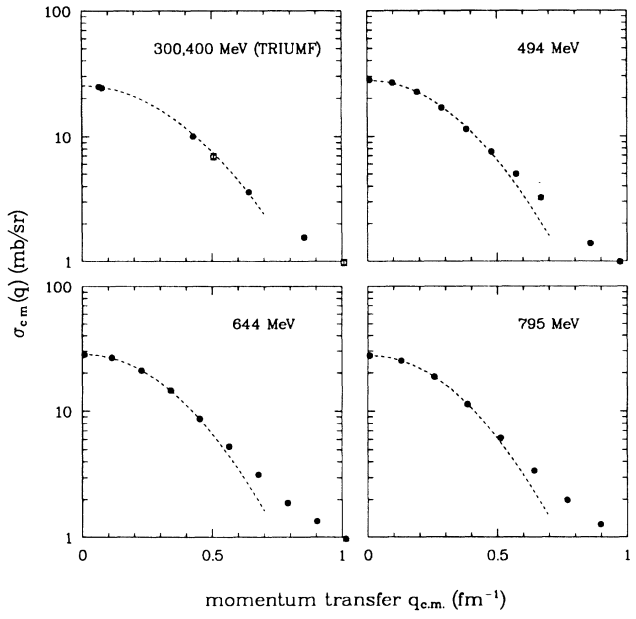


FIG. 7. Low-momentum-transfer differential cross sections for the $^7$Li$(p,n)^7$Be (g.s.+0.43-MeV) reaction at 300 and 400 MeV (TRIUMF, Ref. 14), 494, 644, and 795 MeV. The data for the three highest energies were obtained at LAMPF. The dashed lines for the LAMPF energies correspond to Gaussian least-squares fits to the data for $q \leq 0.5$ fm$^{-1}$.

TABLE I. Zero-momentum-transfer c.m. cross sections for the $^7$Li$(p,n)^7$Be (g.s.+0.43-MeV) transition. The first column (a) corresponds to normalizations based upon a total cross section parametrized as $\sigma_T = e^a E_p^b$ [Eq. (1)]. The second column (b) corresponds to a normalization based upon the parametrization $\sigma_T = (2\pi/k_i k_f) I_q$ [Eqs. (4)–(6)].

| Energy (MeV) | $\sigma_0$ (a) (mb/sr) | $\sigma_0$ (b) (mb/sr) |
|---|---|---|
| 80 | 28.9±1.6 | 26.3±1.6 |
| 120 | 27.6±0.9 | 26.1±0.9 |
| 160 | 26.9±0.7 | 26.0±0.8 |
| 200 | 26.0±0.7 | 25.6±0.7 |
| 494 | 27.0±1.0 | 27.8±0.8 |
| 644 | 27.4±1.1 | 28.3±0.8 |
| 795 | 26.8±1.1 | 27.6±0.8 |

too large will result in a fit that underpredicts the value for $\sigma_0$. Trial fits to calculated cross-section distributions[22] indicate that the momentum-transfer range should be restricted to approximately $q \leq 0.4$ fm$^{-1}$ to avoid underpredicting $\sigma_0$ by more than 1%. This criterion is very nearly satisfied in the present analysis (Figs. 6 and 7).

The zero-momentum-transfer cross sections $\sigma_0$ obtained from the Gaussian fits are displayed in Fig. 8 and Table I. Two sets of data points are plotted: One set corresponds to normalizing to the total-cross-section parametrization of Eqs. (4)–(6) (solid circles); the other corresponds to the parametrization of Eqs. (1) and (2) (open squares). The latter data points have been offset by +5 MeV from the nominal beam energy for plotting clarity. The error bars represent the quadrature combination of the integration uncertainty, the Gaussian fitting uncertainty for $\sigma_0$, and the uncertainty in the total cross sec-

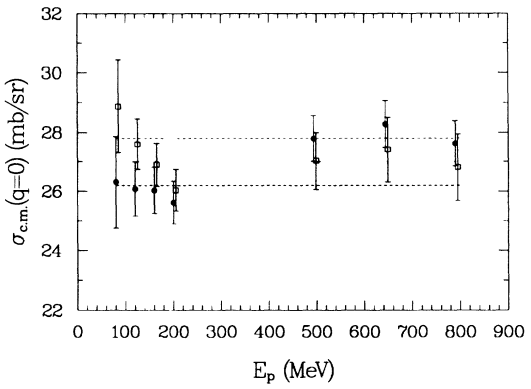


FIG. 8. Zero-momentum-transfer cross sections (c.m.) obtained from Gaussian fits to the experimental cross-section distributions. The solid circles correspond to normalization based upon a constant value for $I_q$ [Eq. (5)]. The open squares correspond to normalization based upon the parametrization of Eq. (1). The dotted line corresponds to a constant c.m. cross section $\sigma_0 = 27.0 \pm 0.8$ mb/sr. The dashed lines represent the one standard deviation limits.

tion. This overall uncertainty is typically 3–6 %.

The shape differences in the momentum-transfer distributions that are derived from Gaussian fitting are not readily apparent in the normalized distributions displayed in Figs. 3 and 4. This qualitative invariance suggests an alternate approach to extracting a "benchmark" cross-section value from the data. The data can be treated as a statistical sample of a single distribution. A polynomial representation of this distribution can then be obtained by a least-squares fit to all the data points. A single value for the integral $I_q$ and the cross section $\sigma_0$ can then be extracted from this fit.

Coefficients for Fourier-Bessel representations of the normalized experimental distributions of $\sigma(q)$ and $q\sigma(q)$ have been obtained by least-squares fitting of the data in Figs. 3 and 4. The cross-section distribution can be described by an expansion in terms of the Bessel function of order zero:

$$\sigma(q)=\sum_{j=1}^{N} a_{0j}J_0(z_{0j}q/q_{\rm lim}) , \tag{9}$$

where

$$J_0(z_{0j})=0 \tag{10}$$

and

$$\sigma(q=0)=\sum_{j=1}^{n} a_{0j} . \tag{11}$$

Similarly, the integrand of $I_q$ can be represented by an expansion in terms of the first-order Bessel function:

$$q\sigma(q)=\sum_{j=1}^{N} a_{1j}J_1(z_{1j}q/q_{\rm lim}) , \tag{12}$$

where

$$J_1(z_{1j})=0 \tag{13}$$

and

$$I_q=\sum_{j=1}^{N} a_{1j}\left[\frac{q_{\rm lim}}{z_{1j}}\right][1-J_0(z_{1j})] . \tag{14}$$

The momentum-transfer limit was chosen to be $q_{\rm lim}=2.6$ fm$^{-1}$. The zeros $z_{0j},z_{1j}$ of the Bessel functions were obtained from the tabulations of Watson.[23] Coefficients obtained from fitting the data with a nine-term expansion are displayed in Table II.

The global Fourier-Bessel fit to the $q\sigma(q)$ distribution can in principle be applied to the individual data sets as an improved means of estimating the cross-section integrand beyond the range of the measured data. However, for the data considered here, the resulting change in the total-cross-section integral is $\leq 1\%$ in all cases. The original exponential estimate (Sec. IV) has therefore been retained.

After normalizing the Fourier-Bessel integral of Eq. (14) to the activation value of Eq. (6), the result $\sigma_0=27.0\pm0.8$ is obtained from Eq. (9). Comparison of this result to the data points in Fig. 8 indicates that this global value is probably not the best representation of the data in specific energy regions. For example, in the energy range 80–200 MeV, the data points normalized to constant $I_q$ [Eq. (6)] have a weighted average of $\sigma_0=25.9\pm0.4$ mb/sr. In the range 490–795 MeV, the weighted average is $\sigma_0=27.9\pm0.4$ mb/sr.

TABLE II. Coefficients for the Fourier-Bessel expansions of $\sigma(q)$ and $q\sigma(q)$ displayed in Figs. 3 and 4. The coefficients $a_{1j}$, when used in Eq. (14), yield a result that is smaller than the activation value [Eq. (6)] by a factor of 1.025. The sum of the coefficients $a_{0j}$ [Eq. (11)], when multiplied by this factor, yields the c.m. cross section $\sigma_0=27.0\pm0.8$ mb/sr.

| $j$ | $a_{0j}$ (mb/sr) | $a_{1j}$ (0.1 fm) |
|---|---|---|
| 1 | 3.264 | 1.596 |
| 2 | 5.055 | 1.808 |
| 3 | 5.256 | 1.745 |
| 4 | 4.722 | 1.851 |
| 5 | 3.508 | 1.503 |
| 6 | 2.260 | 0.9746 |
| 7 | 1.359 | 0.6523 |
| 8 | 0.7066 | 0.4202 |
| 9 | 0.2536 | 0.2393 |

## VI. SUMMARY

The total cross section for the reaction $^7$Li$(p,n)^7$Be (g.s. +0.43 MeV) has been parametrized in two different ways, both of which give equally good fits to the data in the energy range 80–480 MeV. Differential-cross-section distributions for the reaction at 80, 120, 160, 200, 494, 644, and 795 MeV have been integrated and normalized to the parametrized total cross sections. Zero-degree cross sections derived from the normalized distributions are consistent with those obtained in a similar analysis by Watson *et al.*[14] for $E_p \leq 400$ MeV. Laboratory-frame zero-degree cross sections from the present analysis, from the work of Watson *et al.*,[14] and from selected work at lower energies[7,24–26] are displayed in Fig. 9. The dashed line in this figure represents a constant c.m. cross section of 27.0 mb/sr. Above 400 MeV, the zero degree lab cross section appears to rise gradually.

The results for $E_p > 480$ MeV are based upon extrapolations of the total-cross-section data and must be treated with some caution until activation measurements are made for this higher-energy region. However, the approximate invariance of the shape of the differential-cross-section distribution makes it unlikely that the total cross section for this reaction will vary significantly from the extrapolated values. The statistical uncertainty in the extrapolated values is currently less than 4%.

Zero-degree cross sections obtained from an earlier analysis of our 120-, 160-, and 200-MeV distributions were previously reported in Ref. 17. The cross sections plotted in Fig. 16 of that reference are approximately 38 mb/sr, compared to the value of approximately 35 mb/sr represented by the corresponding data points in Fig. 9. This 8% decrease can be attributed partly to the different

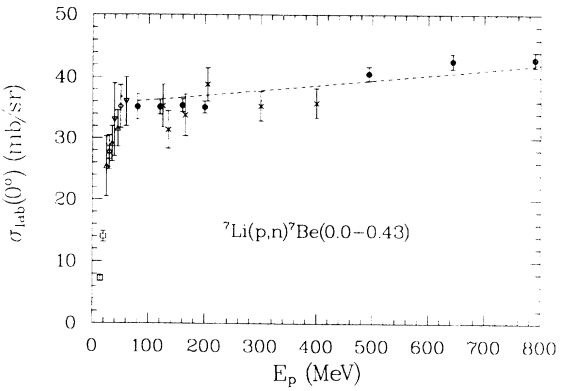


FIG. 9. Laboratory-frame zero-degree differential cross sections. The solid data points are from the present analysis and correspond to normalization based upon a constant value for $I_q$. The dashed line corresponds to a constant c.m. differential cross section of 27.0 mb/sr. The cross sections reported by Watson *et al.* in Ref. 14 (crosses) for $E_p = 120$, 160, and 200 MeV have been offset by +5 MeV for clarity. The lower-energy data points are from Ref. 7 (up triangles; 24.8, 35, and 45 MeV), Ref. 24 (squares; 14.3, 19.4, and 29.6 MeV), Ref. 25 (diamonds; 30 and 50 MeV), and Ref. 36 (down triangles; 39 and 60 MeV).

parametrization of the total cross section (cf. Fig. 8), partly to an improved integration of the experimental cross-section distributions, and partly to the use of the fitted value $\sigma_0$ rather than the single data point $\sigma(0°)$ for each distribution.

Based on consideration of the additional data of Watson *et al.*,[6] the standard laboratory-frame zero-degree cross section adopted in Ref. 17 for the energy range 120–200 MeV was 37 mb/sr. If the Fourier-Bessel c.m. cross section of 27 mb/sr is adopted as the current standard, then the present and previous normalizations in this energy range (where $\sigma_{c.m.}/\sigma_{lab} \simeq 0.74$) are essentially identical. In any case, the range of possible normalizations obtained from the three different treatments represented in Fig. 8 should be a good indication of the systematic uncertainty involved. Extension of the $^7$Li activation measurements to energies larger than 500 MeV should eventually help in adopting a preferred set of normalized cross sections.

## ACKNOWLEDGMENTS

We would like to acknowledge the assistance of R. Alarcon, D. E. Bainum, M. B. Greenfield, D. Krofcheck, D. Mercer, T. Masterson, T. P. Welch, D. Wang, and T. E. Ward in various aspects of the data acquisition. This work was supported in part by the U.S. Department of Energy, the National Science Foundation, the Robert A. Welch foundation, and the Danish Natural Science Research Council.

[1] R. A. Cecil, B. D. Anderson, and R. Madey, Nucl. Instrum. Methods **161**, 439 (1979).
[2] W. C. Sailor, R. C. Byrd, and Y. Yariv, Nucl. Instrum. Methods **A277**, 599 (1989).
[3] P. T. Debevec, G. L. Moake, and P. A. Quin, Nucl. Instrum. Methods **166**, 467 (1979).
[4] S. Cierjacks, M. T. Swinhoe, L. Buth, S. D. Howe, F. Raupp, H. Schmitt, and L. Lehmann, Nucl. Instrum. Methods **192**, 407 (1982).
[5] C. A. Goulding, M. B. Greenfield, C. C. Foster, T. E. Ward, J. Rapaport, D. E. Bainum, and C. D. Goodman, Nucl. Phys. **A331**, 29 (1979).
[6] J. W. Watson, B. D. Anderson, A. R. Baldwin, C. Lebo, B. Flanders, W. Pairsuwan, R. Madey, and C. C. Foster, Nucl. Instrum. Methods **215**, 413 (1983).
[7] S. D. Schery, L. E. Young, R. R. Doering, Sam M. Austin, and R. K. Bhowmik, Nucl. Instrum. Methods **147**, 399 (1977).
[8] J. B. McClelland, Can. J. Phys. **65**, 633 (1987).
[9] C. D. Goodman, J. Rapaport, D. E. Bainum, and C. E. Brient, Nucl. Instrum. Methods **151**, 125 (1978); C. D. Goodman, J. Rapaport, D. E. Bainum, M. B. Greenfield, and C. A. Goulding, IEEE Trans. Nucl. Sci. **NS-25**, 577 (1978).
[10] C. D. Goodman, C. C. Foster, M. B. Greenfield, C. A. Goulding, D. A. Lind, and J. Rapaport, IEEE Trans. Nucl. Sci. **NS-26**, 2248 (1979).
[11] L. Valentin, G. Albouy, J. P. Cohen, and M. Gusakow, Phys. Lett. **7**, 163 (1963); Nucl. Phys. **62**, 81 (1965).
[12] T. E. Ward, C. C. Foster, G. E. Walker, J. Rapaport, and C. A. Goulding, Phys. Rev. C **25**, 762 (1982).
[13] J. D'Auria, M. Dombsky, L. Moritz, T. Ruth, G. Sheffer, T. E. Ward, C. C. Foster, J. W. Watson, B. D. Anderson, and J. Rapaport, Phys. Rev. C **30**, 1999 (1984).
[14] J. W. Watson, R. Pourang, R. Abegg, W. P. Alford, A. Celler, S. El-Kateb, D. Frekers, O. Hausser, R. Helmer, R. Henderson, K. Hicks, K. P. Jackson, R. G. Jeppesen, C. A. Miller, M. Vetterli, S. Yen, and C. D. Zafiratos, Phys. Rev. C **40**, 22 (1989).
[15] F. Ajzenberg-Selove, Nucl. Phys. **A320**, 66 (1979).
[16] F. Ajzenberg-Selove, Nucl. Phys. **A490**, 66 (1988).
[17] T. N. Taddeucci, C. A. Goulding, T. A. Carey, R. C. Byrd, C. D. Goodman, C. Gaarde, J. Larsen, D. Horen, J. Rapaport, and E. Sugarbaker, Nucl. Phys. **A469**, 125 (1987).
[18] M. A. Franey and W. G. Love, Phys. Rev. C **31**, 488 (1985).
[19] R. E. Rand, R. Frosch, and M. R. Yearian, Phys. Rev. **144**, 859 (1966); **148**, 1246(E) (1966).
[20] L. R. Suelzle, M. R. Yearian, and H. Crannell, Phys. Rev. **162**, 992 (1967).
[21] G. J. C. Van Niftrik, L. Lapikás, H. DeVries, and G. Box, Nucl. Phys. **A174**, 173 (1971).
[22] J. Rapaport, C. C. Foster, C. D. Goodman, C. A. Goulding, T. N. Taddeucci, D. J. Horen, E. R. Sugarbaker, C. Gaarde, J. Larsen, J. A. Carr, F. Petrovich, and M. J. Threapleton, Phys. Rev. C **41**, 1920 (1990).
[23] G. N. Watson, *Theory of Bessel Functions* (Cambridge Univer-

sity Press, Cambridge, 1952), p. 748.
[24]M. W. McNaughton, N. S. P. King, F. P. Brady, J. L. Romero, and T. S. Subramanian, Nucl. Instrum. Methods **130**, 555 (1975).
[25]C. J. Batty, B. E. Bonner, A. I. Kilvington, C. Tschalar, L. E. Williams, and A. S. Clough, Nucl. Instrum. Methods **68**, 273 (1969).
[26]J. W. Wachter, R. T. Santoro, T. A. Love, and W. Zobel, Nucl. Instrum. Methods **113**, 185 (1973).